PROCEEDINGS OF SCIENCE

Light (anti)nuclei production in small systems

Rutuparna Rath* **(for the ALICE collaboration)**

[a] *Istituto Nazionale di Fisica Nucleare, Sezione di Bologna, Via Irnerio 46, Bologna, Italy*

E-mail: rutuparna.rath@cern.ch

Over the past decade, the ALICE experiment has extensively measured the production of light (anti)nuclei. Despite a wealth of experimental findings, the mechanism behind the production of these particles remains enigmatic, raising intense debate within the scientific community. Typically, experimental data are interpreted using two distinct phenomenological models: the statistical hadronization model and baryon coalescence. This contribution will offer an overview of recent ALICE findings regarding measurements of light (anti)nuclei production. These measurements will be discussed in the broader context of available phenomenological models, aiming to construct a comprehensive understanding. This contribution outlines the prospects for advancing this line of research during the LHC Run 3.

11th Edition of the Large Hadron Collider Physics Conference
22th - 26th May 2023
Faculty of Physics and Institute of Physics of the University of Belgrade, Belgrade, Serbia

*Speaker

PoS(LHCP2023)134

1. Introduction

Measuring light (anti)nuclei formed in high-energy hadronic collisions offers valuable insights into their creation mechanisms, a pivotal inquiry in heavy-ion physics. Two distinct model classes exist to elucidate the observed production outcomes: the Statistical Hadronization Model (SHM) and the coalescence models. In the SHM [1], hadrons emerge from a source in thermal equilibrium, with their abundances predetermined during chemical freeze-out. Conversely, the genesis of light (anti)nuclei is attributed to the coalescence of protons and neutrons occupying proximal positions in phase space during kinetic freeze-out, aligning in spin to form nuclei [2]. The key observable of this model is the coalescence parameter $B_{\rm A}$. If A is the mass number of the formed nucleus, this parameter is defined as

$$B_{\rm A} = \frac{\left(\frac{1}{2\pi p_{\rm T}^{\rm A}}\frac{d^2N}{dydp_{\rm T}^{\rm A}}\right)}{\left(\frac{1}{2\pi p_{\rm T}^{\rm p}}\frac{d^2N}{dydp_{\rm T}^{\rm p}}\right)^{\rm A}}, \tag{1}$$

where the invariant spectra of (anti)protons is evaluated at the reduced transverse momentum $p_{\rm T}^{\rm p} = p_{\rm T}^{\rm A}/A$. This parameter's calculation involves assessing the overlap between the nucleus wave function and the constituents' phase space distribution through the Wigner formalism [3], determining the production probability of the nucleus. In ALICE, we have studied the production spectra of (anti)deuterons, (anti)^{3}H, and (anti)^{3}He in small collision systems such as pp and/or p–Pb collisions at several energies. The ALICE apparatus is constituted by detectors placed at central rapidities (which is also called as central barrel) and forward detectors. For the (anti)nuclei identification, we use the Inner Tracking System (ITS), the Time Projection Chamber (TPC) and the Time of Flight (TOF) detectors. In the next section, we will discuss important findings in the small collision systems which also serve as a baseline/reference to study the large collision systems such as Pb–Pb and Xe–Xe, etc.

2. Results and discussion

Throughout the LHC's Run 1 and Run 2, ALICE conducted successful (anti)nuclei analyses utilizing data gathered from pp and p–Pb collisions [4], particularly for (anti)nuclei with atomic mass numbers (A) below 4. As LHC's Run 3 continues, capitalizing on the extensive statistical data available, we can enhance the precision of these measurements while also expanding our analyses to include heavier (anti)nuclei. In Figs. 1a and 1b, we have shown the transverse momentum ($p_{\rm T}$) spectra and corresponding coalescence probability distribution as a function of $p_{\rm T}$/A of (anti)^{3}He obtained in different multiplicity classes for p–Pb collision system at $\sqrt{s_{\rm NN}}$ = 5.02 TeV, respectively [5]. As we can observe that the coalescence parameter is almost flat for all the multiplicity classes except for minimum bias events it shows an increasing trend while going towards higher $p_{\rm T}$/A.

The ratio between the measured yields of nuclei and that of protons is sensitive to the light nuclei production mechanism. In Figs. 2a and 2b the yield ratio to protons for deuterons and ^{3}He as a function of average charged particle multiplicity is shown in pp, p–Pb and Pb–Pb collisions [4, 6–8] and compared to the expectations of the models. A smooth increase of this ratio with the charged particle multiplicity is observed, reaching a constant value in Pb–Pb collisions. The two ratios show a similar trend with average charged particle multiplicity, however, the increase from

pp to Pb–Pb results is about a factor of 3 larger for ^{3}He/p than for d/p. The observed evolution of the d/p ratio is well described by the coalescence approach because of the increasing phase space in Pb–Pb. For high charged-particle multiplicity densities, the coalescence calculations and the canonical statistical model (CSM) expectations are close and both describe the behaviour of the data, within the current uncertainties. On the other hand, the models struggle to describe the ratio to protons for nuclei with A=3, as it is clear in Figure 2b.

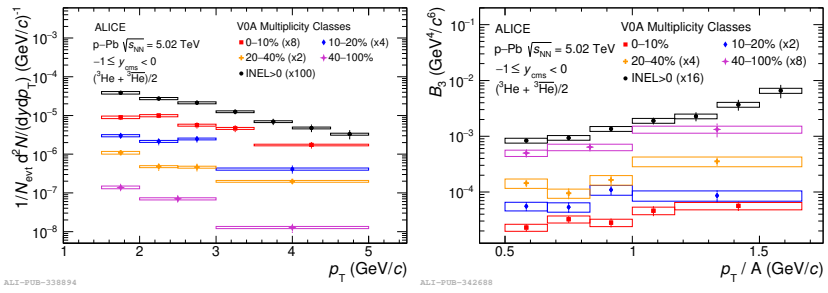

(a) (b)

Figure 1: (a) Transverse momentum spectra and (b) coalescence parameter (B_3) of ^{3}He in p–Pb collisions at $\sqrt{s_{NN}}$ = 5.02 TeV for different multiplicity classes [5].

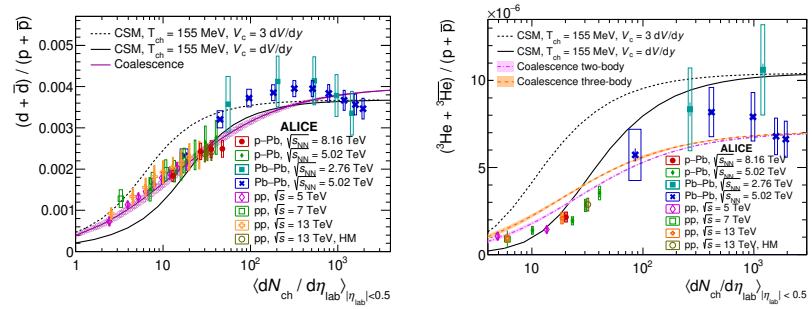

(a) (b)

Figure 2: The yield ratio to protons for (a) deuterons and (b) ^{3}He as a function of average charged particle multiplicity is shown in pp, p–Pb and Pb–Pb collision systems [4, 6–8].

Figures 3a and 3b illustrate the variation of coalescence parameters B_2 and B_3 with the charged-particle multiplicity, at a given p_T/A value. These measurements depict a gradual shift from low charged-particle multiplicities, indicative of smaller system sizes, toward larger ones. The declining pattern observed in B_2 and B_3 with increasing charged particle multiplicities implies a continuous evolution of the production mechanism from smaller to larger systems. This suggests a single mechanism, sensitive to system size, potentially governing the production of nuclei. The theoretical calculations demonstrate qualitative alignment with the trends observed in the experimental data.

An alternative approach to validate the coalescence model involves examining the coalescence parameter within small systems, both inside and outside of jets. Jets in small systems, compared to larger ones like Pb–Pb, typically exhibit nucleons closer in phase space. Consequently, the coalescence model predicts a heightened coalescence parameter within jets compared to the underlying event. A high-p_T particle (specifically, $p_T > 5$ GeV/c) serves as a proxy for the jet axis. Using the cumulative distribution function (CDF) technique, three azimuthal regions of equal width are identified: Toward (containing the jet and underlying event), Away (with the recoil jet and underlying event), and Transverse (dominated by the underlying event). By subtracting spectra of the Transverse region from the Toward region, the jet contribution is derived, which is depicted in Fig. 4a. Figure 4b showcases results for the deuteron coalescence parameter in pp collisions at

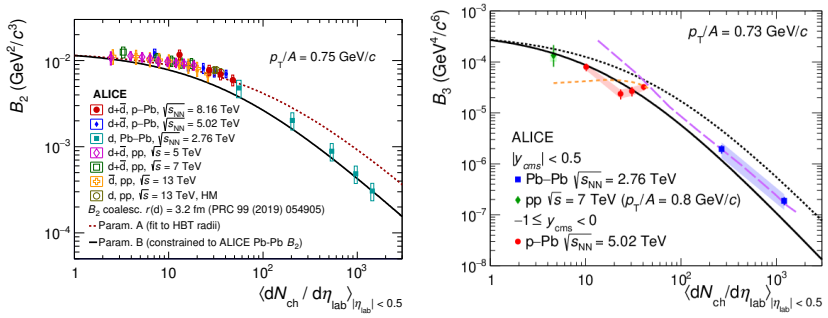

(a) (b)

Figure 3: The variation of coalescence parameters (a) B_2 and (b) B_3 with the charged-particle multiplicity are presented at a given p_T/A value [9, 10].

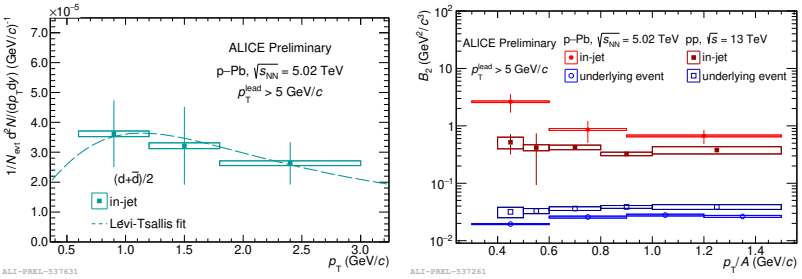

(a) (b)

Figure 4: (a) Transverse momentum spectra with jet contribution is shown for (anti)deuterons in p–Pb collisions at $\sqrt{s_{\rm NN}}$ = 5.02 TeV. (b) Coalescence parameter B_2 in and out of jets in pp collisions at $\sqrt{s}$ = 13 TeV (darker points) [11] and in p–Pb collisions at $\sqrt{s_{\rm NN}}$ = 5.02 TeV (brighter points) as a function of the reduced transverse momentum.

$\sqrt{s}$ = 13 TeV [11] and p–Pb collisions at $\sqrt{s_{\rm NN}}$ = 5.02 TeV. An enhancement of B_2^{jet} compared to B_2^{UE} is evident in both collision scenarios, with a notably wider gap observed in the p–Pb system. The underlying event results align well with the coalescence model: given that the p–Pb system has a larger source size than pp (1.5 fm [12] versus 1 fm [13]), a smaller coalescence parameter is anticipated in p–Pb compared to pp. However, for the in-jet aspect, the larger B_2 in p–Pb jets could be due to particles being closer in phase space than in the pp system, though further investigations are warranted, as the particle composition within jets might also influence coalescence probability.

3. Summary and outlook

The coalescence approach accounts for experimental findings encompassing the ratio of integrated yields for nuclei and protons, alongside the coalescence parameter, $B_{\rm A}$, relative to the charged-particle multiplicity density at midrapidity. At higher charged-particle densities, both the coalescence approach and the CSM effectively explain the d/p ratio. However, models struggle to accurately represent the ratio to protons for nuclei with A=3. To enhance precision, more refined measurements will leverage data from the ongoing ALICE Run 3 campaign. Furthermore, upcoming phenomenological calculations aim to enhance the theoretical comprehension of (anti)nuclei production mechanisms in ultrarelativistic heavy-ion collisions.

References

[1] A. Andronic, P. Braun-Munzinger, J. Stachel and H. Stocker, Phys. Lett. B **697**, 203 (2011).

[2] S. T. Butler and C. A. Pearson, Phys. Rev. **129**, 836 (1963).

[3] F. Bellini and A. P. Kalweit, Phys. Rev. C **99**, 054905 (2019).

[4] J. Adam *et al.* [ALICE], Phys. Rev. C **93**, 024917 (2016).

[5] S. Acharya *et al.* [ALICE], Phys. Rev. C **101**, 044906 (2020).

[6] S. Acharya *et al.* [ALICE], Phys. Lett. B **794**, 50 (2019).

[7] S. Acharya *et al.* [ALICE], Phys. Lett. B **800**, 135043 (2020).

[8] S. Acharya *et al.* [ALICE], Phys. Rev. C **97**, 024615 (2018).

[9] S. Acharya *et al.* [ALICE], JHEP **01**, 106 (2022).

[10] S. Acharya *et al.* [ALICE], Phys. Lett. B **846**, 137795 (2023).

[11] S. Acharya *et al.* [ALICE], Phys. Rev. Lett. **131**, 042301 (2023).

[12] S. Acharya *et al.* [ALICE], Phys. Rev. Lett. **123**, 112002 (2019).

[13] S. Acharya *et al.* [ALICE], Phys. Rev. C **99**, 024001 (2019).